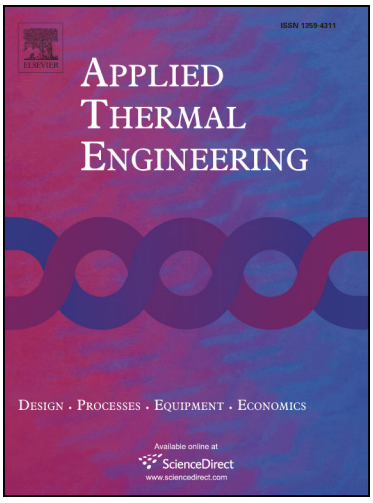

Low melt alloy blended polyalcohol as solid-solid phase change material for energy storage: an experimental study

KP Venkitaraj, B Praveen, Harjit Singh, S Suresh

PII: S1359-4311(19)32887-X
DOI: https://doi.org/10.1016/j.applthermaleng.2020.115362
Reference: ATE 115362

To appear in: *Applied Thermal Engineering*

Received Date: 30 April 2019
Revised Date: 9 April 2020
Accepted Date: 15 April 2020

Please cite this article as: K. Venkitaraj, B. Praveen, H. Singh, S. Suresh, Low melt alloy blended polyalcohol as solid-solid phase change material for energy storage: an experimental study, *Applied Thermal Engineering* (2020), doi: https://doi.org/10.1016/j.applthermaleng.2020.115362

Low melt alloy blended polyalcohol as solid-solid phase change material for energy storage: an experimental study

K P Venkitaraj[a, b], B Praveen[a] , Harjit Singh[c] ,S Suresh[a,*]

[a] *Department of Mechanical Engineering, National Institute of Technology, Tiruchirappalli-620015, India*

[b] *Department of Mechanical Engineering, College of Engineering, Adoor-691551, India*

[c]*Brunel University London, Kingston Lane Uxbridge, Uxbridge UB8 3PH, UK*

* Corresponding Author

Dr. K P Venkitaraj

Research Scholar

Department of Mechanical Engineering

National Institute of Technology Tiruchirappalli, India.

Email: venkitaraj@cea.ac.in

Mob: +91 9496500422

Mr. B Praveen

Research Scholar

Department of Mechanical Engineering

National Institute of Technology Tiruchirappalli, India.

Email: praveennitt15@gmail.com

Mob: +91 8848625935

Dr. S Suresh

Assistant Professor

Department of Mechanical Engineering

National Institute of Technology Tiruchirappalli, India.

Email: ssuresh@nitt.edu

Mob: +919489066246

Dr. Harjit Singh

Senior Lecturer

Mechanical and Aerospace Engineering

Howell Building 131,Brunel University,

Middlesex, Uxbridge, UK.

Email: harjit.singh@brunel.ac.uk

Tel**:** +44 (0) 1895 265468

Low melt alloy blended polyalcohol as solid-solid phase change material for energy storage: an experimental study

K P Venkitaraj[a, b], B Praveen[a] , Harjit Singh[c] , S Suresh[a*]

[a] Department of Mechanical Engineering, National Institute of Technology, Tiruchirapalli, Tamilnadu, 620015, India

[b] Department of Mechanical Engineering, College of Engineering Adoor, Kerala, 691551, India

[c] Brunel University London, Kingston Lane Uxbridge, Uxbridge UB8 3PH, UK

*Corresponding author Email address: ssuresh@nitt.edu (S Suresh)

Abstract

This paper reports the results of the experimental study conducted on the charging and discharging performance of a pentaerythritol (PE) blended with the low melt alloy (LMA) of Bi-Sn-In-Zn. The charging and discharging time, power, the efficiency of PE added with 0.5, and 1.0 wt.% of LMA determined using a shell and tube type thermal energy storage system. Therminol-55 oil, a heat transfer fluid in hot and cold conditions was circulated at 2, 4, 6 LPM through the heat exchanger during the charging and discharging processes. The results indicated that charging and discharging time reduced due to the blending of LMA with PE for all volume flow rates of therminol oil. The maximum charging and discharging powers of 265.9 W and 187.0 W respectively were observed in the case of PE+1.0% LMA corresponding to the flow rate of 6 liters per minute (LPM). The efficiencies of charging and discharging showed maximum values of 82.5% and 69.0% respectively at 6 LPM. The mean value of the overall energy efficiency of the thermal energy storage system found increased from 38.3% obtained in the case of PE to 45.2 % and 51.6% obtained for PE added with 0.5 wt. % and 1.0 wt. % of LMA respectively.

Keywords: Pentaerythritol, low melt alloy, charging and discharging, overall energy efficiency, solid-solid PCM.

Abbreviations

PCM	phase change material
LMA	low melt alloy
HTF	heat transfer fluid
PE	pentaerythritol
DSC	differential scanning calorimetry
LPM	liter per minute
TES	thermal energy storage
SSPCM	solid-solid PCM

Notations and Symbols

T	temperature, °C
t	time of discharge, minute/second
Q	heat, kJ
h	specific enthalpy, kJ/kg
m_p	mass of the PCM, kg
$\dot{m}$	mass flow rate of the HTF, kg/s
c_p	specific heat, kJ/kg-K
η	efficiency, %

1. Introduction

The gap between supply and demand for energy considerably can be reduced by employing an efficient energy storage system. Use of Phase Change Material (PCM) for thermal energy storage and building cooling is getting attention in the recent years [1, 2]. The latent heat storage systems using PCM are more efficient than sensible heat storage systems because of the high-energy storage density. Moreover, the energy storage process occurs at constant temperature in the latent heat systems [3]. The organic PCM is more chemically stable than inorganic PCM, and the super cooling is not a big issue in them [4]. The thermal and chemical stability of PCM is to be ensured before selecting them for long-run thermal energy storage applications. [5-7]. Many solid-liquid PCM that are employed for energy storage applications suffer from volume expansion and leakage problems in their liquid phase [8]. There exists a few PCM such as shape-stabilized PCMs that are not exhibiting these kinds of issues. Again, these limitations can be eliminated by using a solid-solid PCM (SSPCM). SSPCM exhibits transition from one crystal structure to another at elevated temperature accompanied by the absorption/release of the tremendous amount of heat [9]. Polyhydric alcohols such as pentaerythritol, pentaglycerine, and neopentyl glycol are SSPCM having heat of transition as good as to the latent heats of several solid-liquid PCM [10-11]. Numerous investigations on polyhydric alcohols as probable SSPCM have been reported in the literature [12-15]. Barrio et al. [16] reported the mechanisms of solid-solid transition in polyhydric alcohols and commented that polyhydric alcohols undergo sub cooling or super cooling during the discharging process. The super cooling cause the reformation of the hydrogen bonds during the discharging process to occur at a lower temperature than the temperature at which breaking of the bonds occurs during the charging process.
The majority of PCM, in general, has a very poor thermal conductivity which results in lower charging and discharging rates. The literature reported the use of thermally conductive particles like nanoparticles as additives to enhance the thermal energy storage performance of organic and inorganic PCM [17-19]. The research findings also indicated that the enhancement of thermal conductivity accompanied by a slight decrease in the phase change properties of PCM [20]. Siegel [21] investigated the use of high conductivity particles to enhance the rate of solidification molten salt. He reported an enhancement of 17% in the rate of energy transfer using 20% volume of the particles. The composites PCM comprising graphite widely experimented due to its high thermal conductivity. Cabeza et al. [22] and Py et al. [23] studied PCM/graphite enclosed in waterlogged metal modules. They observed a heat barrier between the metal modules and water. Yin et al. [24] experimented paraffin/expanded graphite composite and reported that the thermal conductivity enhanced about 17 fold compared to the thermal conductivity of pure paraffin. Kim and Drzal [25] reported that the presence of conductive graphite affects the phase change properties of PCM. Elgafy and Lafdi [26] studied the performance enhancement of paraffin/ carbon nanofibres (CNF) with the mass fraction of CNF varied between 1 and 4%. Tun-Ping Teng and Chao-Chieh Yu [27]

prepared composite PCM comprising paraffin and 1.0, 2.0, and 3.0 wt. % of Al_2O_3, TiO_2, SiO_2 nanoparticles. Their study revealed that TiO_2 enhances the thermal performance of paraffin more efficiently compared to other nanoparticles. Zhiwei Ge et al. [28] tested composite PCM comprising carbonate-salt for medium and high-temperature energy storage applications. Xiang Li et al. [29] investigated calcium chloride hexahydrate with aluminum oxide nanoparticles for thermal energy storage. D K Singh et al. [30] experimentally studied the thermal energy storage performance of Myo-Inositol based nano PCM. They used Myo-Inositol added with 1%, 2% and 3% mass fractions of CuO and Al_2O_3 nanoparticles. Based on the results of DSC, TGA, and FTIR analysis, they commented that the nano-enhanced myo-inositol is a potential PCM for thermal energy storage.

M. Ghalambaz et al. [31] numerically studied the melting behaviour of nanoparticles enhanced phase change materials in an enclosure using hybrid nanoparticles. They reported that hybrid nanoparticles composed of Mg–MgO showed enhanced fusion performance. N. H. Boukani et al. [32] numerically investigated Melting of a NePCM in partially filled horizontal elliptical capsules. They employed n-octadecane paraffin dispersed with Cu nanoparticles in their numerical study. In another study, Praveen and Suresh [33] investigated the thermal percolation effect of Low Melt alloy (LMA) of Bi Sn Zn In in the mico-encapsulated PCM. They concluded that the presence of conductive particles enhances the melting rate and decreases the volume change of NePCM as compared to the pure PCM.

Though there are numerous investigations reported on solid-liquid PCM, the papers on thermal energy storage performance of SSPCM with heat transfer enhancement additives are decidedly less in number. P.Hu et al. [34] studied solid state phase transition of pentaerythritol (PE) added with nano-aluminum nitride. In our recent work [35] we studied the thermal and chemical stability of PE added with 0.1 wt. % of metal oxide nanoparticles. We found that the nanoparticles decreased the sub cooling effect during the cooling cycle. We have also investigated the energy storage characteristics and crystallization kinetics of PE added with indium, a low melting metal [36].

We [37] in our another paper reported the charging and discharging performance of pentaerythritol added with Al_2O_3 nanoparticles using the IC engine exhaust gas using a shell and tube heat exchanger and observed that the addition of 0.1 wt. % and 0.5 wt. % of Al_2O_3 nanoparticles enhances the charging and discharging efficiency of PE. In one of our previous study [38], we confirmed the thermal and chemical stability of PE blended with low melting alloy (LMA) for its possible use as PCM for Latent Heat Storage. The results reported indicated that the addition of 0.1 and 0.5 wt. % does not alter the thermal and chemical stability of PE during cyclic heating and cooling. In this paper, we reported the results of the experimental investigation of the charging and discharging performance of PE added with 0.5 wt. % and 1.0 wt. % of LMA using thermal energy storage (TES) system comprising a shell and tube heat exchanger.

The charging and discharging efficiencies and the overall energy efficiency of the TES for different volume flow rates of the heat transfer fluid (HTF) reported.

2. Experimental

2.1 Materials

Pentaerythritol (PE) is the PCM used for conducting the experiments reported in this paper. PE is a solid-solid organic material showing an enthalpy change of about 260 kJ/kg during its transition from one crystal structure to another. At normal temperature, PE has a body centered tetragonal crystal structure. When the material is heated, the crystal structure changes to face centered cubic at a fixed temperature. This process is associated with absorption of thermal energy. During the cooling process, the material regains its original structure and this process is associated with the release of stored thermal energy. Figure 1 shows the solid-solid transition taking place in a PE molecule. In the PE molecule (figure 1 (a)), the central carbon atom is surrounded by four methylenic carbon atoms forming a tetrahedral structure. At normal ambient conditions, PE has a body-centered tetragonal (BCT) structure in which the molecules are linked together by hydrogen bonds along the (001) planes as shown in figure 1(b). The different molecular layers are linked together through weak Van der waals forces acting along the crystallographic axis (figure 1(c)). At higher temperatures (solid-solid transition temperature), the crystal structure of PE changes to face-centered cubic crystalline structure (FCC) and this phase transition is accompanied with the absorption of heat. Figure 1(d) shows the FCC structure of PE. Pentaerythritol (98.0% pure) in powder form supplied by Alfa Easer, USA.

Figure 2(a) shows the XRD pattern of PE obtained using Bruker AXS D8 Advance X-ray diffractometer having Cu-kα1 radiation in the range of 0–90◦. The reflections in the XRD pattern obtained were recognized as matching to the tetragonal phase of PE using JCPDS (Joint Committee on Powder Diffraction Standards). The SEM analysis was performed using Jeol JSM 6390LV SEM to study the microstructure of PE. The obtained SEM image showed that PE has a loose microstructure with large number of individual lamellae on the surface (Figure 2 (b)).

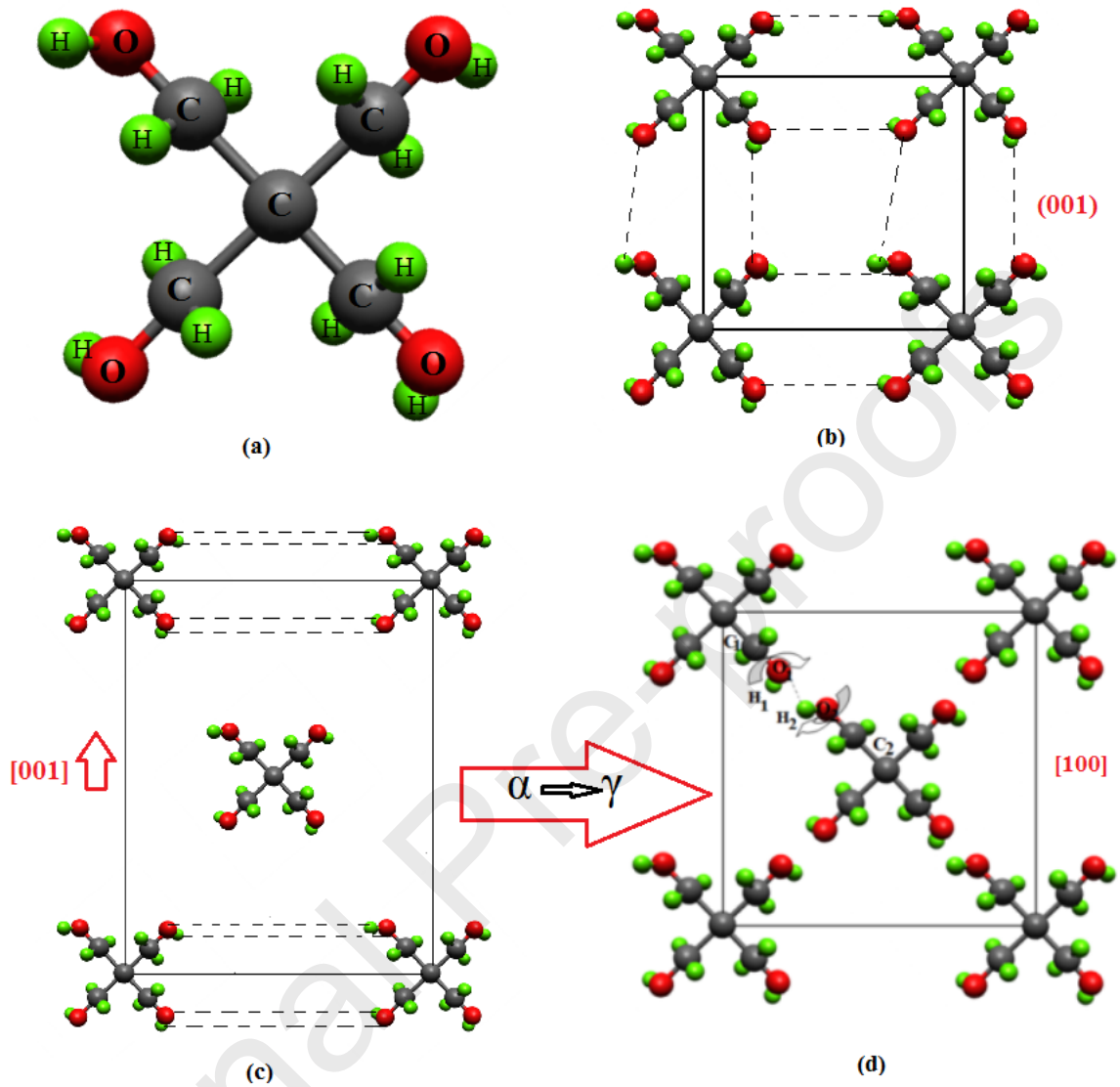

Figure 1: (a) Atomic arrangement in a PE molecule, Legend: carbon, black; oxygen, red; hydrogen, green (b) BCT structure of PE projected down the b-axis. (c) BCT structure of PE projected down c-axis. (d) FCC structure of PE with intermolecular bond rotation. Dashed lines mark the hydrogen bonds. Solid lines represent the unit cell.

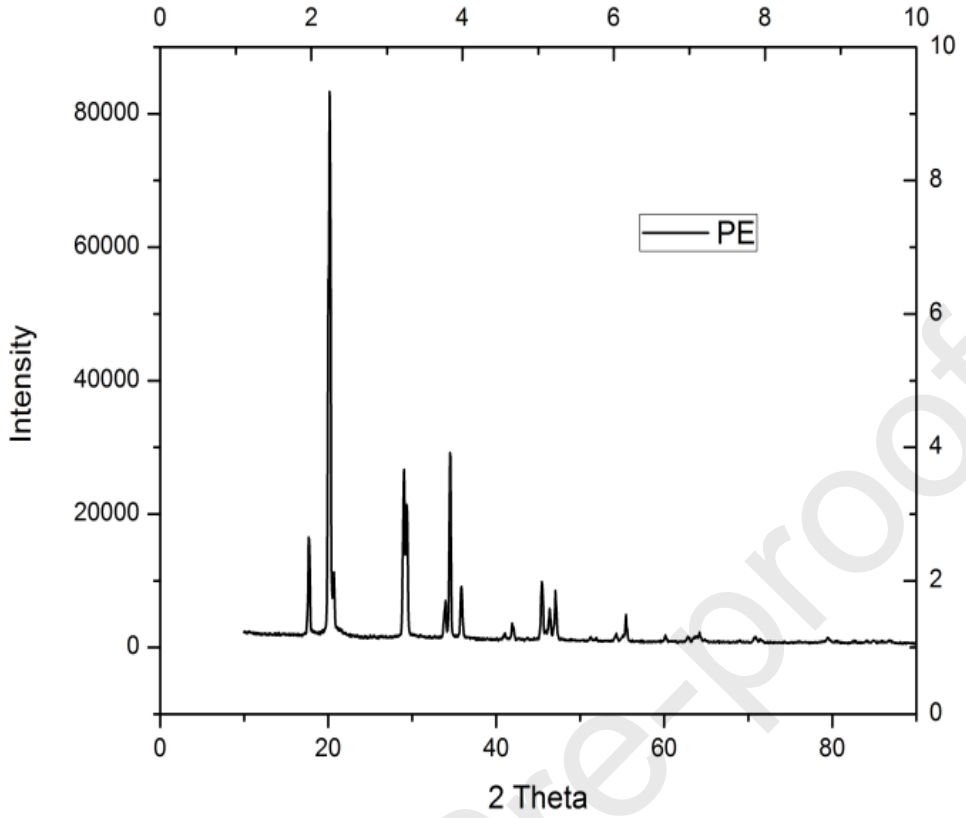

(a)

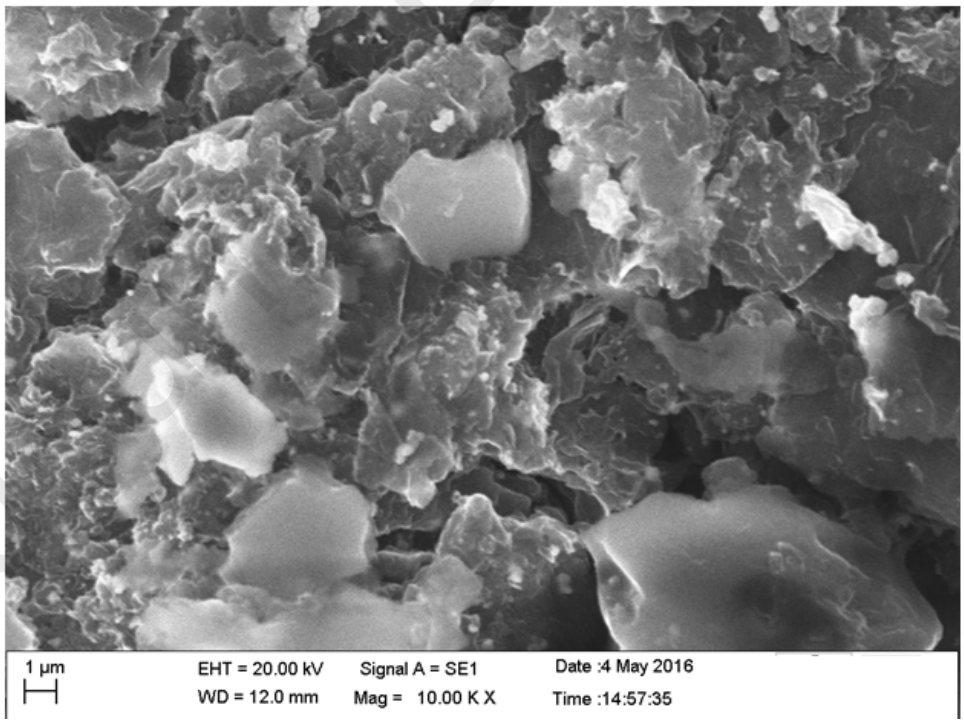

(b)

Figure 2: (a) XRD pattern of PE, (b) SEM image of PE

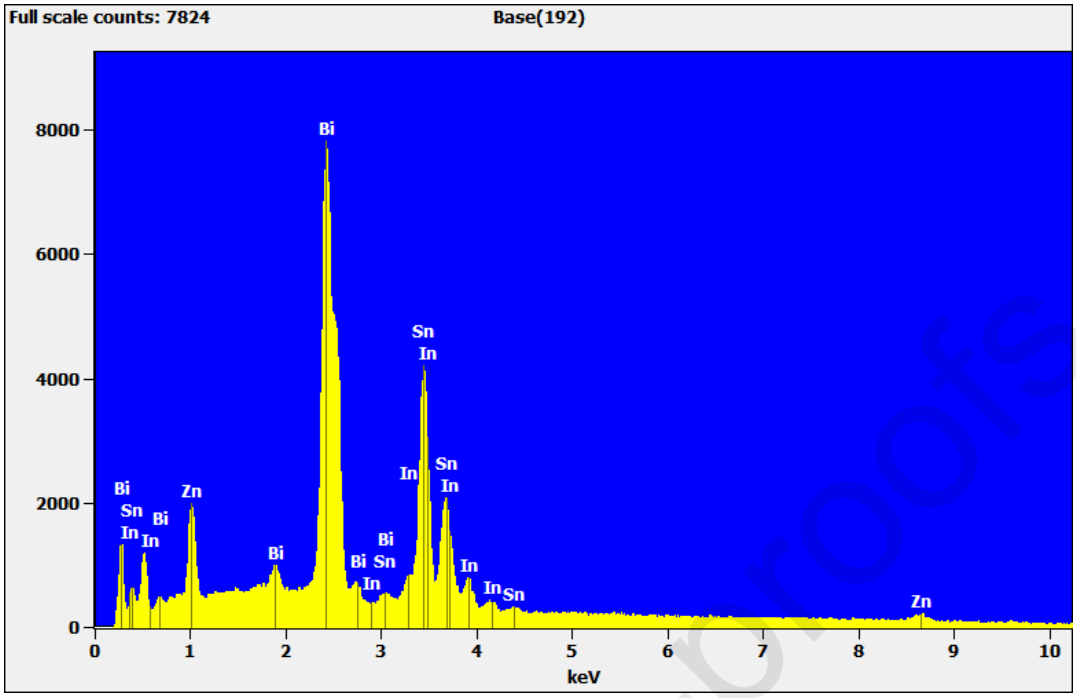

Figure 3: EDS spectra of Low Melt Alloy

The choice of PE as a PCM for thermal energy storage is limited by its low thermal conductivity. Therefore, thermally conductive additives can be used to enhance the thermal conductivity of PE. In this experimental work, we have tested the suitability of a low melt alloy composed of bismuth (Bi), indium (In), zinc (ZN) and tin (Sn) for enhancing the thermal conductivity of PE. Saru Metals Pvt Ltd, India supplied the LMA in the form of ingot. The alloy has the melting temperature in the range 121-131°C. The LMA ingot converted into powder form by using a grinding machine. More refined powder produced with help of the ball. The composition of the LMA is confirmed as Bi(32%), Sn(59%), In(5%), Zn(4%) by analyzing the Energy Dispersive Spectroscopy (EDS) spectra of the LMA (figure 3). The therminol-55 is the heat transfer fluid (HTF) used for the charging and discharging process.

3. Methodology

3.1 Preparation of PE/LMA composite PCM

The experimental charging and discharging performance are carried out using PE/LMA composite PCM containing 0.5, and 1.0 wt. % of LMA. A uniform mixture of PE and the LMA obtained using a ball mill run at 200rpm for 1.5 hrs.

3.2 Thermal property measurement of PE/LMA

3.2.1. Thermal conductivity and specific heat

T-history method [39] used to estimate the thermal conductivity and specific heat of the PE/LMA samples. The detailed procedure of the T-history method explained in our

previous work. The measurements were made over a temperature regime ranging from 30℃ to 210℃. The whole temperature range is divided into six small intervals as, (i) 30-60℃ (average temperature =45℃), (ii) 60-90℃ (average temperature =75℃), 90-120℃ (average temperature =105℃),120-150℃ (average temperature =135℃),150-180℃ (average temperature =165℃) and 180-210℃ (average temperature =195℃). The thermal conductivity and specific heat values of the samples in these intervals were estimated using T-history data. Figure 4 shows the variation of the thermal conductivity and specific heats of samples with temperature. The average values of thermal conductivity and specific heat of pure PE over the entire temperature range of 30℃ to 210℃ were estimated as 0.106W/m-K and 2.78 kJ/kg-K respectively. The avearge thermal conductivity increased to 0.123 W/m-K, and 0.140 W/m-K respectively corresponding to 0.5 and 1.0 wt. % of LMA. The results also showed that the average specific heat decreased to 2.72 kJ/kg-K and 2.66 kJ/kg-K when 0.5 wt. % and, 1.0 wt. % LMA respectively added to PE. It can be noted that the LMA used in this work has a melting temperature in the range 121-131°C. This implies that LMA will be in molten state above ~121 and 131°C during the charging and discharging processes, thus allowing liquid alloy to infiltrate between particles of phase change materials thereby imparting increased thermal conductivity.

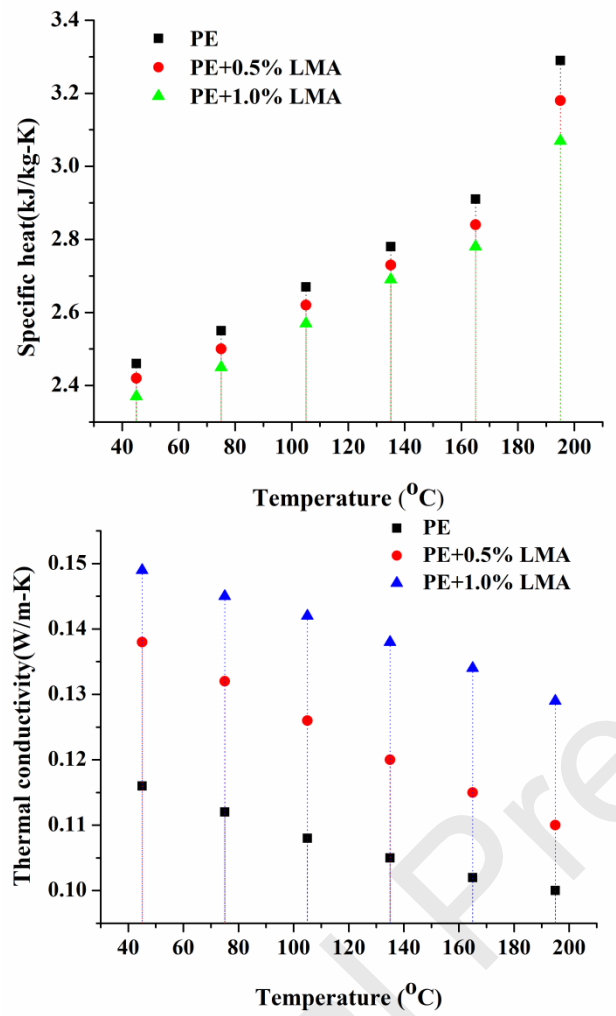

Figure 4: Variation of thermal conductivity and specific heat of PCM with temperature

3.2.2. Enthalpy of solid-solid transition

The heat of solid transition of the PE/LMA composite PCM measured by Differential Scanning Calorimetry (DSC) method. The PCM samples are subjected to heating and cooling between the temperature range 30-280°C at 10°C/min. An inert atmosphere of Argon was used during the heating and cooling of the samples in order to prevent oxidation of the PCM samples.

The DSC instrument details are given in table 1.

Table 1: Specifications of DSC equipment

Make and Model	Mettler Toledo DSC 822e, Hong Kong
Range	Temperature. -130 °C to 450°C Measurement ± 350 mW at room temperature
Resolution	0.04 mW at room temperature

Accuracy	± 0.2°C
Reproducibility	± 0.1°C

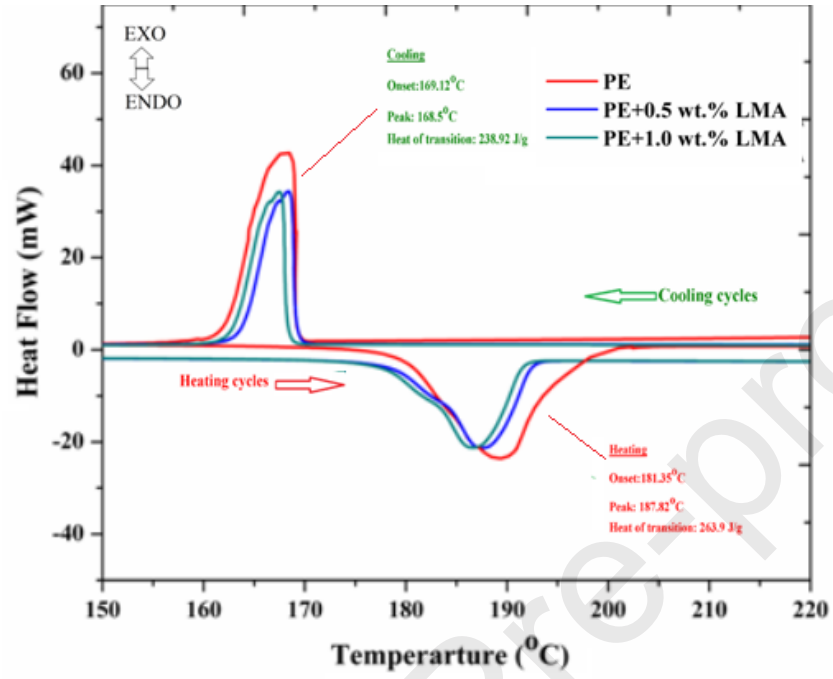

Figure 5: DSC curves of the PCM samples

Figure 5 shows the DSC curves obtained for the PCM samples. The solid to solid phase transition in PE during heating cycle started at 181.4 °C, reached its peak at 187.8 °C and it ended at 193.6 °C. During this solid state phase transition 263.9 kJ/kg heat absorbed by the PE. During the cooling cycle, the reverse phase transition began at 169.1 °C, showed its peak at168.6 °C and it ended at 163 °C. The heat released during the reverse phase transition obtained as 238.9 kJ/kg. In the case of PE+0.5 wt.% LMA, the phase transition in PE during heating cycle started at 183.9°C, showed its peak at 187.6°C and the it ended at 192.3°C. The heat absorbed by PE+0.5 wt. % LMA during this solid state phase transition found as 246.9 kJ/kg. During the cooling of PE+0.5 wt. % LMA, the reverse phase transition began at 169.0 °C, showed its peak at168.5 °C and it ended at 163.1 °C. The heat released during the cooling cycle obtained as 212.9 kJ/kg.

The solid to solid phase transition in PE+1.0 wt. % LMA during the heating observed between the temperatures 183.7°C and191.7°C respectively and the peak of this phase transition occurred at 187.2°C. The heat of absorption during this charging process found as 243.1 kJ/kg. During the discharge cycle, the solid to solid transition started at 169.6°C and it ended at 162.9°C. The peak of this transition happened at 167.8°C. The heat released during this phase transition calculated as 207.3 kJ/kg.

3.3 Experimental setup

The thermal energy storage performance of pentaerythritol added with different heat transfer enhancement additives were tested by conducting charging and discharging experiments using a thermal energy storage system. The schematic diagram of the experimental setup shown in figure 6. The experimental setup comprises a shell and tube type heat exchanger filled with the PCM. The shell side of the heat exchanger filled the PCM tested for thermal energy storage performance. The fluid flowing through the copper tubes exchanges heat with the PCM during the charging and discharging process. The hot thermal fluid from the hot fluid container is pumped through the heat exchanger using a gear pump. The flow rate of the hot thermal fluid is controlled using a bye pass valve provided in the delivery side of the gear pump. A rotameter is provided to monitor the flow rate of hot therminol flowing through the heat exchanger. The hot fluid after flowing through the copper tubes flows back to the hot reservoir. During the flow through the heat exchanger, the hot fluid loses its heat to the PCM surrounding the copper tubes. This is the charging cycle of the experiment. The cold line of the experimental setup consists of a cold fluid container centrifugal pump; rotameter, and an air-cooled heat exchanger. During the discharge cycle, the cold thermal fluid is pumped through the heat exchanger using the centrifugal pump. The flow rate of the cold fluid is monitored and controlled by using a rotameter and a valve provided in the delivery side of the centrifugal pump. The cold fluid flowing through the copper tube receives heat stored by the PCM. The cold fluid leaving from the other end of the heat exchanger flows back to the cold reservoir via a radiator. During the flow through the radiator, it loses heat. The temperature of the fluid entering and leaving the heat exchanger is monitored and recorded by using the calibrated K-type thermocouples. The temperature of the PCM inside the shell at the leading end, middle and, trailing ends are also monitored using the K-type thermocouples. A multi-channel data logger records the PCM and the fluid temperatures during the charging and discharging process.

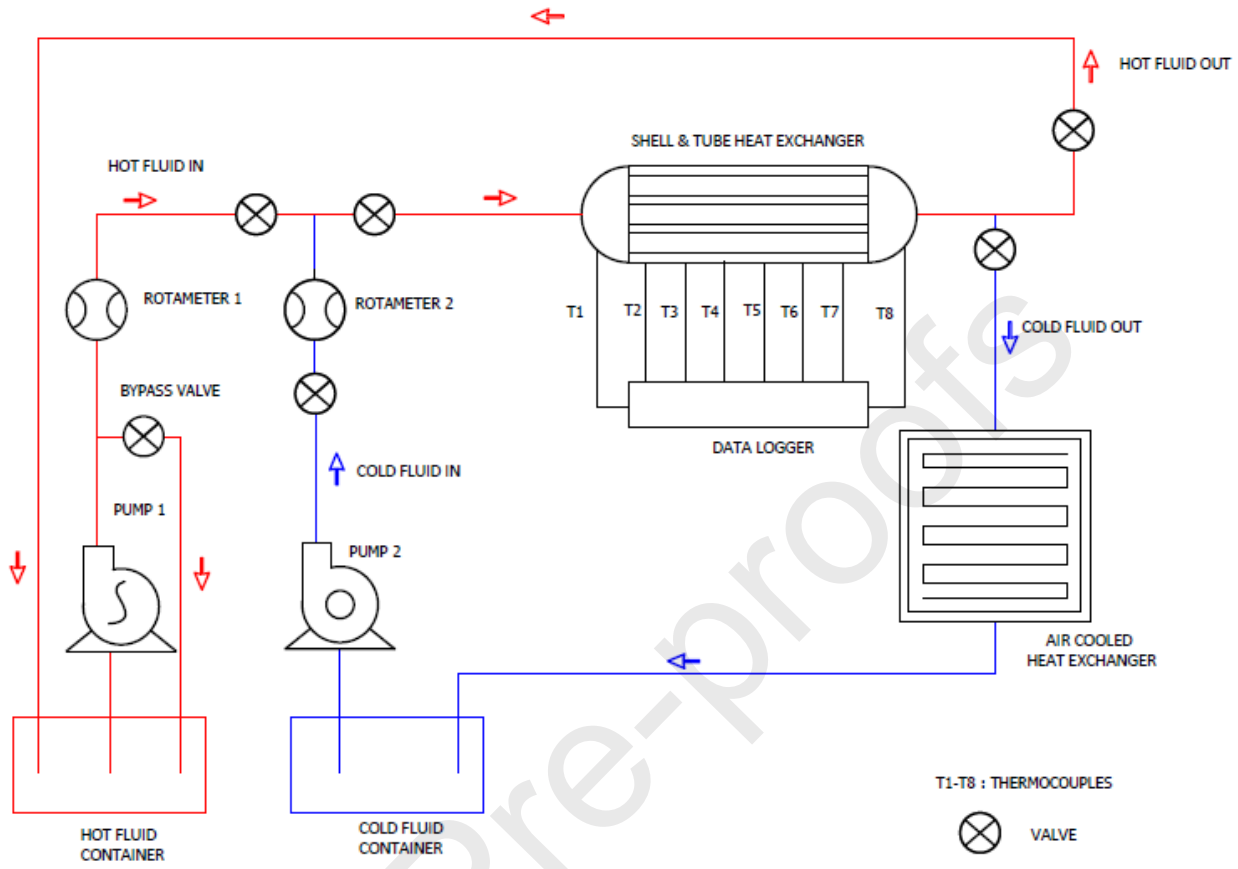

Figure 6: Schematic diagram of the experimental setup for heat transfer study

Figure 7 shows the constructional features of the shell and tube heat exchanger. The heat exchanger comprises three tubes of 20 mm inner diameter, 2mm thickness, and 45 cm effective length enclosed within a shell of 65 mm inner diameter, and 5 mm thickness. The tubes are made of copper and the shell is made of mild steel. The shell insulated using glass wool and asbestos in order to minimize the heat loss to the surroundings. The quantity of PCM required for filling in the space inside the shell estimated as 1.22 kg. The heat transfer fluid used in the hot and cold circuits is Therminol 55. The temperature of therminol oil maintained at 200^{o}C by using two hand immersion heaters of 1500W each. The gear pump (Make: HMP pumps, power: 0.5 HP, size: ½" x ½," rpm: 1440, maximum discharge: 30 LPM) was used to pump the hot therminol oil through the heat exchanger. The cold fluid pumped by using a monoblock centrifugal pump (Make: Lakshmi pumps, power: 0.5 HP, size: 1" x 1", rpm: 1400, max. discharge: 45 LPM). The flow rate of hot therminol oil is measured using a metal tube magnetic rotameter (Make: Eureka, model: SSVS-MTS-4, Range: 1.1 to 11 LPM). The flow rate in the cold side of the experimental setup measured by using an acrylic body rotameter (Make: Flow point, range: 1 to 10 LPM). Two metal containers, each 20-liter capacity, were used as hot and cold fluid reservoirs. The entire hot circuit, part of the cold circuit between the heat exchanger exit and radiator inlet are well insulated to minimize the heat loss to the surroundings.

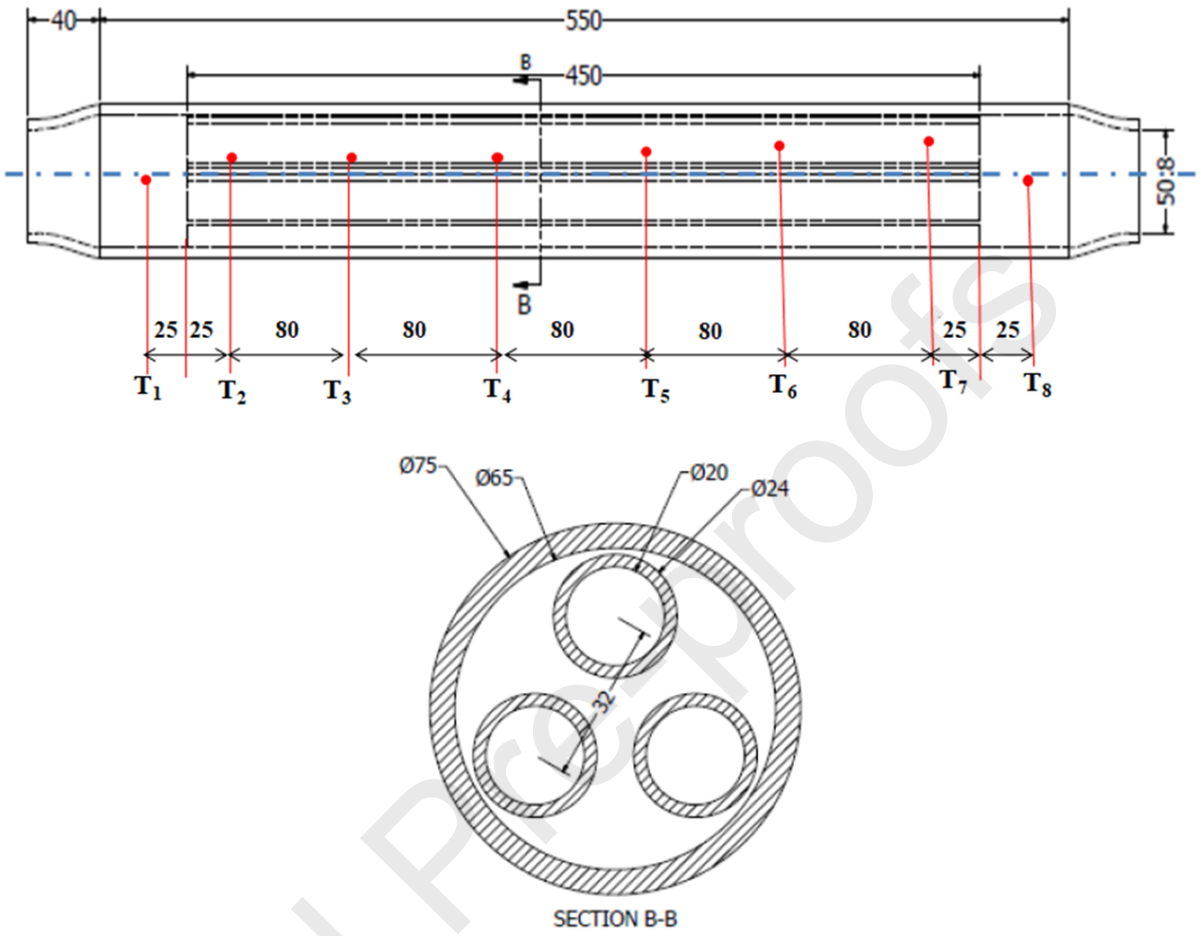

Figure 7: Constructional details of the heat exchanger

3.4 Procedure

The experiments performed using pure PE and PE added with 0.5 and, 1.0 wt.% of LMA. The detailed experimental procedure given below. The heat exchanger filled with pure PE on the shell side mounted in the experimental setup. The heaters in the hot fluid reservoir are switched on to heat the therminol oil above 200^{o}C. The hot therminol oil pumped through the heat exchanger by switching on the gear pump. The flow rate of the oil set at 2 LPM by regulating the bye pass valve. The temperature of the hot therminol entering and leaving the heat exchanger and the PCM temperatures at different locations recorded. The gear pump switched off when the PCM temperature recorded crosses the solid-solid transition temperature of the PCM. This completes the charging process. The cold therminol oil pumped through the heat exchanger by starting the centrifugal pump. The flow rate of the cold therminol adjusted to 2 LPM by operating the valve. The temperature of the cold therminol entering and leaving the heat exchanger and the PCM temperatures at different locations recorded.

The centrifugal pump switched off when the PCM temperature restored to its ambient temperature. This completes the discharging process. The experiment repeated for hot

and cold therminol flow rates of 4 LPM and 6 LPM. The experiment is repeated for PE/LMA composite PCM of 0.5 and 1.0 wt.% LMA.

3.5 Data Reduction

The amount of heat supplied to the PCM is calculated using the equation,

$$Q_{sp} = \dot{m}_h \, c_{p,h} \, (T_{i,h} - T_{o,h}) \, t, \quad kJ \tag{1}$$

where $\dot{m}_h$ is the mass flow rate (kg/s) of hot HTF, $c_{p,h}$ is the specific heat of hot HTF, $T_{i,h}$ and $T_{o,h}$ is the inlet and the exit temperature of the hot HTF, and t is the time of storage.

Heat stored = sensible heat + solid-solid transition heat.

$$Q_{st} = Q_{sen} + Q_{trs} = m_p \, c_{p,\,p} \, (T_{trs} - T_{p.i}) + m_p \, h_{trs}, \quad kJ \tag{2}$$

m_p - the mass of the PCM (pentaerythritol), T_{trs} - solid to solid transition temperature of the PCM, $T_{p,i}$ - initial temperature of the PCM, h_{trs} - enthalpy of transition, $c_{p,\,p}$ is the specific heat of PCM.

Now, charging efficiency is found as the ratio of the heat stored (Q_{st}) by the PCM to the heat supplied (Q_{sp}) by the HTF. i.e.,

$$\text{Charging efficiency (\%)}, \eta_c = \frac{Q_{st}}{Q_{sp}} \text{ x } 100 \tag{3}$$

$$\text{Heat rejected to the cold HTF,} \quad Q_{re} = \dot{m}_c \, c_{p,c} \, (T_{o,c} - T_{i,c}) \, t, \quad kJ \tag{4}$$

Where $\dot{m}_c$ - mass flow rate (kg/s) of cold HTF, $c_{p,c}$ - specific heat of cold HTF, $T_{i,c}$ and $T_{o,c}$ - the inlet and the exit temperature of the cold HTF, and t - time taken for the discharge.

The discharging efficiency determined as the ratio of the amount of heat rejected to the cold HTF (Q_{re}) to the heat stored (Q_{st}) by the PCM, i.e.,

$$\text{Discharging efficiency (\%)}, \eta_d = \frac{Q_{re}}{Q_{st}} \text{ x } 100 \tag{5}$$

The overall energy efficiency of the thermal energy storage (TES) system used in this experimental study calculated by combining the efficiencies computed separately for the charging and discharging processes [40-41].

$$\text{Overall energy efficiency of the TES system, } \eta = \eta_c \text{ x } \eta_d \tag{6}$$

4. Energy Storage and Discharge Analysis

4.1 Charging performance analysis

During the charging process, the HTF (Therminol oil) heated to about 225°C and circulated through the heat exchanger. The PCM temperature variation from the inlet to the exit of the heat exchanger in the axial direction recorded for evaluating the charging

performance of the PCM. Figure 8 shows the temperature variation in the case of pure PE for HTF flow rates of 2, 4, and 6 LPM. T_1 and T_2 represent the variation of HTF temperatures at inlet and exit of the heat exchanger. The variation of the PCM temperature at six locations in the heat exchanger is plotted as T_2 to T_6 in this figure. During the charging process, the PCM in the shell side of the heat exchanger absorbs the heat of the hot HTF. The charging process continued till all the temperatures recorded by the thermocouples crossed the solid-solid transition temperature of pure PE. The charging process ended in 152 minutes when the HTF flow rate of 2 LPM maintained through the heat exchanger. The charging period found decreased to 103 minutes and 68 minutes when the therminol flow rate changed to 4 LPM and 6 LPM respectively. The increase in charging time observed was because of the increased energy supplied at the higher flow rate.

It can be seen from figure 8 that the flat plateau representing the solid-solid transition in PCM is absent in the charging curves. The placement of the temperature sensor and the flow rate of HTF control this phase transition process during the charging and discharging processes. The absence of the flat plateau in the charging curves shown in figure 8 is mainly because of the higher flow rates (2, 4 and 6 LPM) of the HTF maintained in this experimental work. Again, at the lowest flow rate of 2 LPM, a slight bump can be observed in the charging curves of PE. This small bump was observed in the temperature range 180-190℃ and happens to be the temperature range in which solid-solid transition of the PCM occurs.

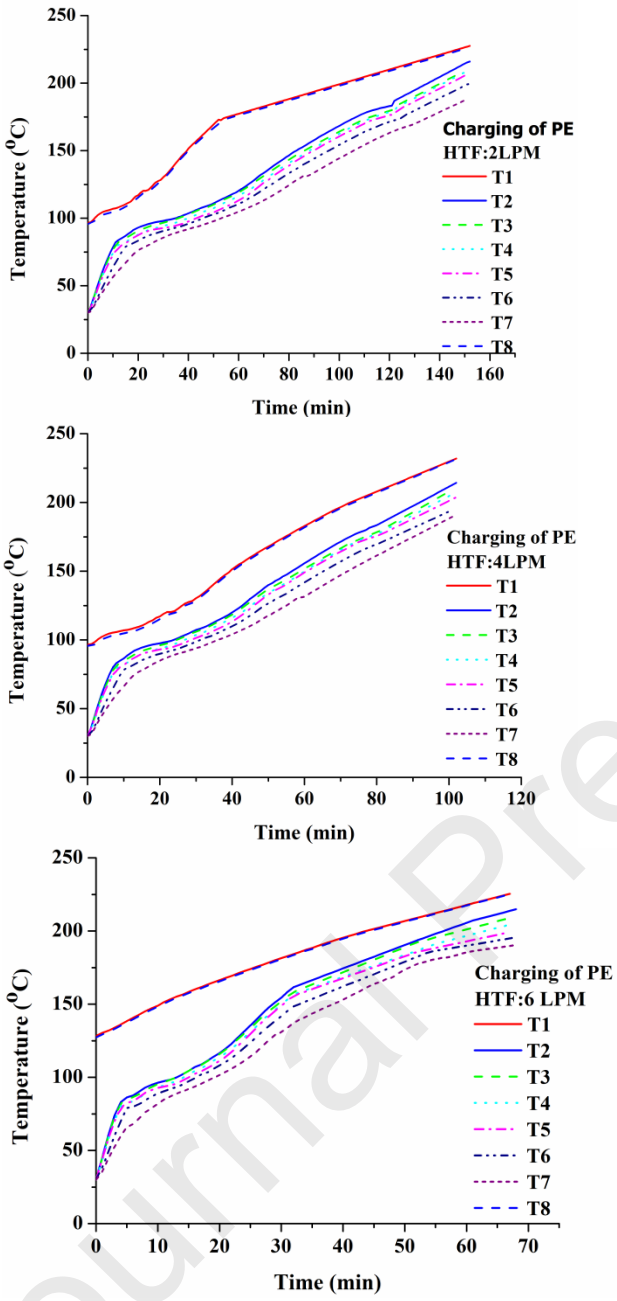

Figure 8: Charging process of pure PE at different flow rates of HTF (T1 & T8-HTF entry & exit temperatures, T2 to T7-PCM temperatures)

Figure 9 shows the effect of adding 0.5 wt. % of LMA on charging performance of PE. The charging of PE+0.5 wt. % LMA finished in 133 minutes when the HTF flow rate of 2 LPM maintained through the heat exchanger. The charging period decreased to 93 minutes and 60 minutes when the HTF flow rates changed to 4 LPM and 6 LPM respectively. Figure 10 shows the effect of adding 1.0 wt. % of LMA on charging performance of PE. The charging of PE+1.0 wt. % LMA finished in 118 minutes when the HTF flow rate of 2 LPM maintained through the heat exchanger. The charging period

decreased to 86 minutes and 54 minutes when the flow rate changed to 4 LPM and 6 LPM respectively.

Figure 11 shows the % reduction in the charging time of PE due to the addition of LMA at different flow rates of the HTF. The graph shows that the charging time of PE decreases due to the addition of 0.5 and 1 wt.% of LMA at all volume flow rates of the heat transfer fluid. The addition of 0.5 wt. % of LMA caused 12.5%, 8.8% and 11.8% reduction in the charging time of PE at the therminol volume flow rates of 2, 4 and 6 LPM respectively. In the case of PE added with 1.0 wt.% of LMA, the charging time of PE reduced by 22.3%, 18.0%, and 20.6% respectively corresponding to the therminol flow rates of 2, 4 and 6 LPM.

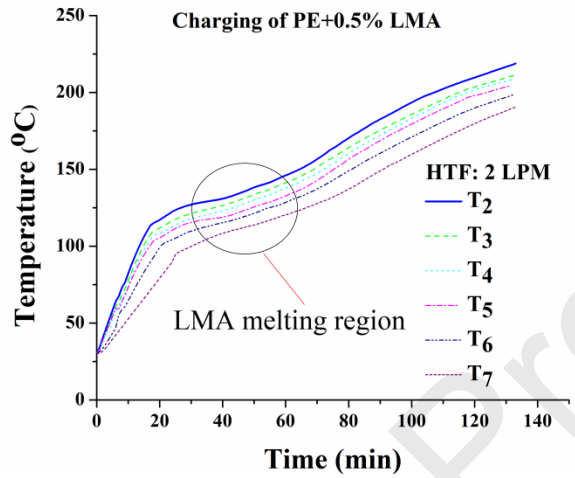

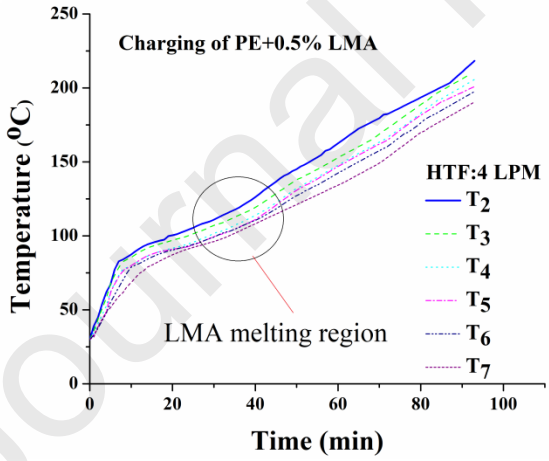

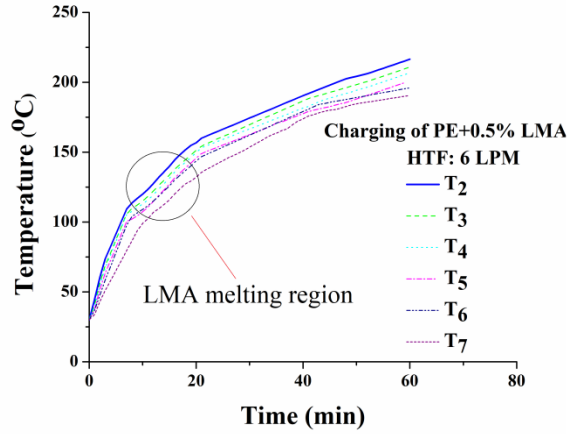

Figure 9: Charging process of PE+0.5 wt. % LMA at different flow rates of HTF (The circled area shows the region where the LMA got melted)

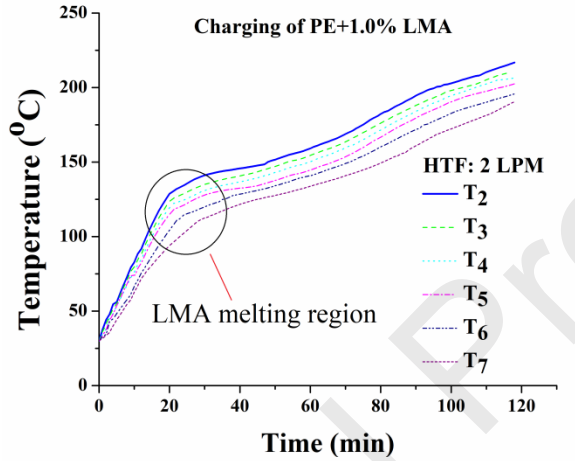

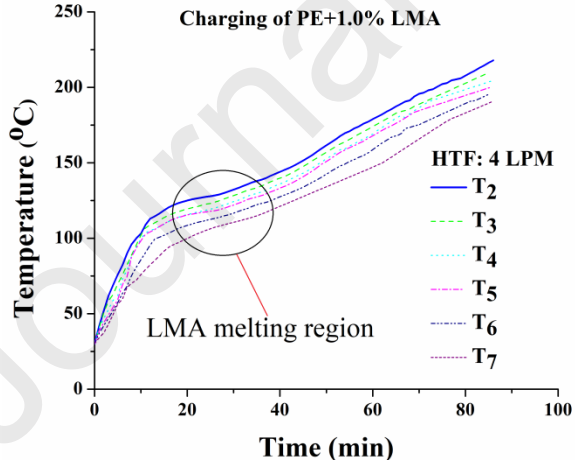

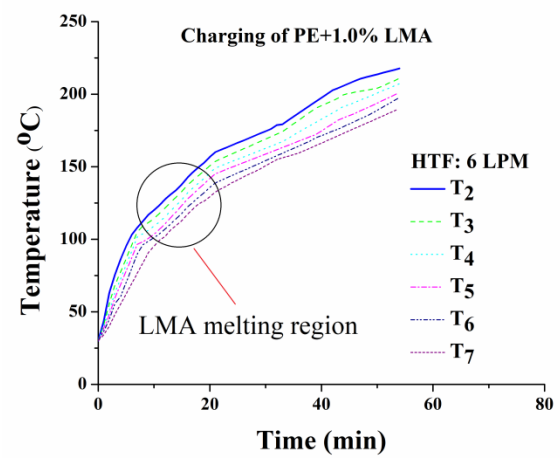

Figure 10: Charging process of PE+1.0 wt. % LMA at different flow rates of HTF (The circled area shows the region where the LMA got melted)

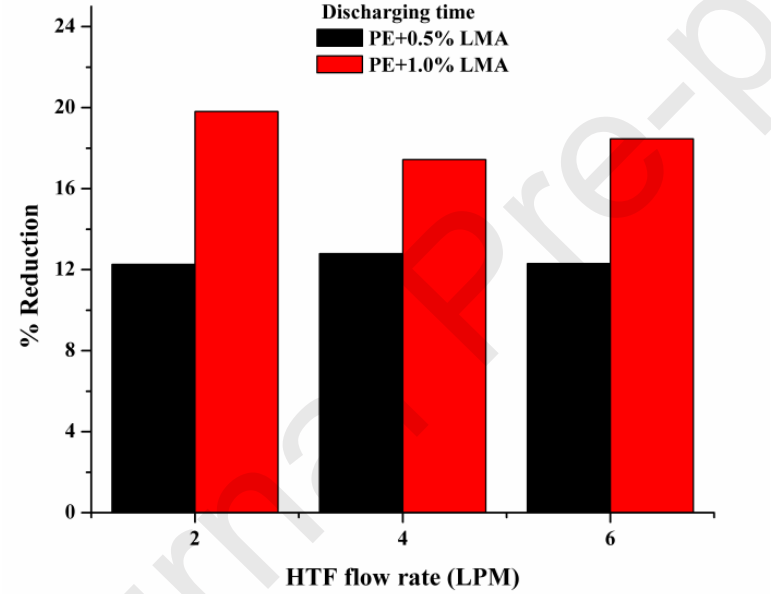

Figure 11: % reduction in charging time of PE due to LMA at different flow rates

4.2 Charging power and charging efficiency at different flow rates.

The average energy stored in unit time estimated as the charging power. Figure 12 given below gives the average charging power estimated in the case of pure PE, and PE added with 0.5 wt. % and 1.0 wt. % of LMA.

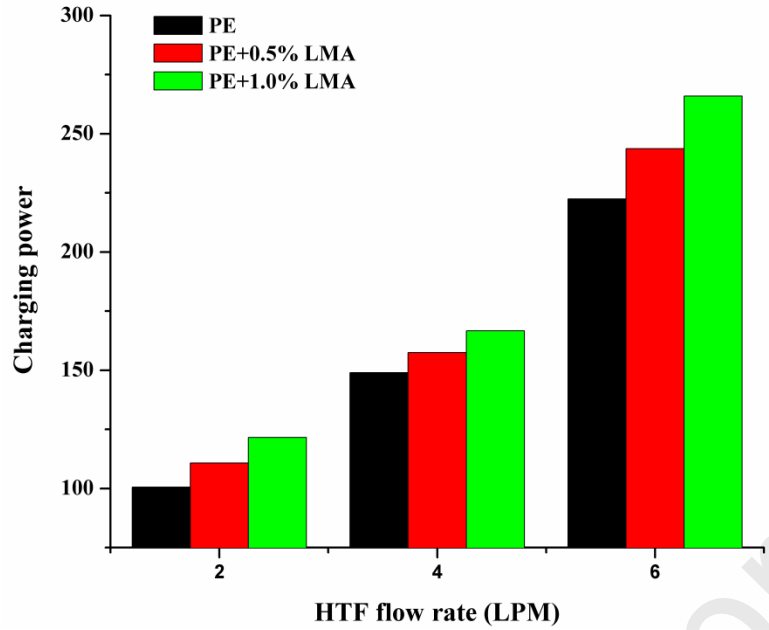

Figure 12: Average charging power at different HTF flow rates

It understood that the charging power of PE increases with the addition of additives for all the heating rates considered in this study. The average energy storage power of pure PE corresponding to 2 LPM, 4 LPM, and 6 LPM flow rates estimated as 100.5 W, 149.0 W, and 222.5 W respectively. The results of the experiment conducted using PE added with 0.5 wt. % of LMA showed the average charging power corresponding to 2 LPM, 4 LPM, and 6 LPM flow rates as 110.8 W, 157.5 W, and 243.7 W respectively. In the case of PE+1.0 wt.% LMA, the average charging power corresponding to 2, 4, and 6 LPM flow rates increased to 121.6 W, 166.7 W, and 265.9 W respectively.

Figure 13 shows the charging efficiency obtained in the case of pure PE and PE added with 0.5 and 1.0 wt. % of LMA at different HTF flow rates. In the case pure PE, an amount of 916.4.kJ energy stored out of the 1418.2 kJ heat supplied at an HTF flow rate of 2 LPM, indicating a charging efficiency of 64.6%. When the flow rate changed to 4 LPM, 911.6 kJ of heat stored out of 1322.8 kJ of heat supplied. This accounts for a charging efficiency of 68.9%. When the flow rate further increased to 6 LPM, the heat supplied and heat stored estimated as 907.8 kJ and 1256.8 kJ showing a charging efficiency of 72.2%.

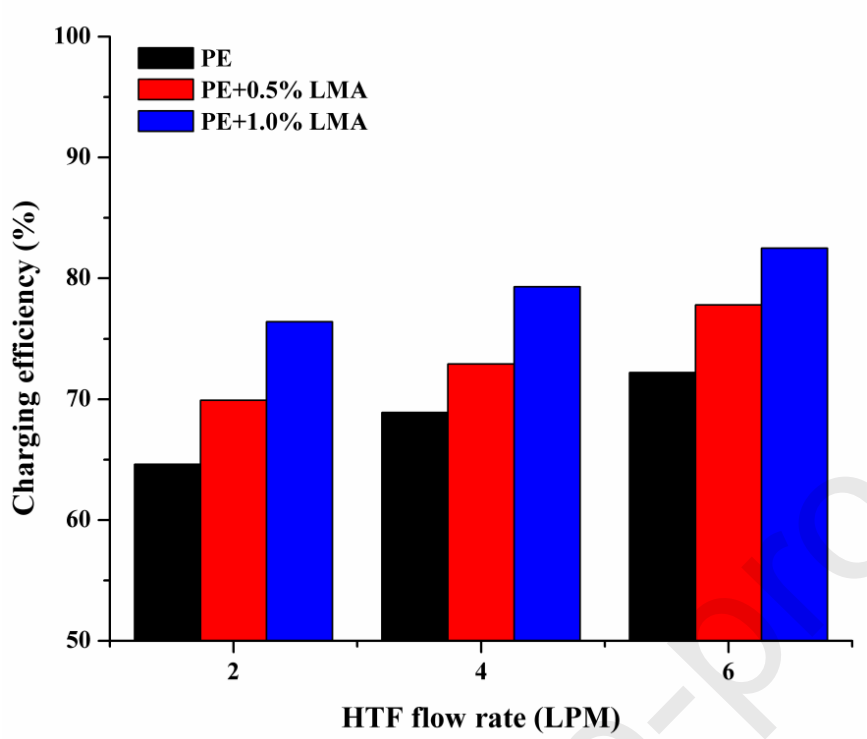

Figure 13: Charging efficiency at different flow rates

Figure 13 also shows the charging efficiency obtained in the case of PE added with 0.5 and 1.0 wt% of LMA and LMM. When 0.5 wt% of LMA added to PE, 884.1 kJ of heat stored out of the 1264.8 kJ of heat supplied indicating a charging efficiency of 69.9% at an HTF flow rate of 2LPM. When the flow rate changed to 4 LPM, 878.7 kJ heat stored by the PCM out of 1206.1 kJ of heat supplied. The charging efficiency at this flow rate obtained as 72.9%.The charging efficiency increased as 77.8% at flow rate 6 LPM. The energy supplied and stored at this flow rate found to be 1128.2 kJ and 877.5 kJ respectively. The experimental results using PE+1.0 wt. % LMA indicated a charging efficiency of 76.4% when a flow rate of 2 LPM maintained through the heat exchanger. The heat supplied and stored at this flow rate found to be 1126.4 kJ and 860.7 kJ respectively. When the therminol flow rate adjusted to 4 LPM, 860 kJ heat stored out of 1084.3 kJ heat supplied. The charging efficiency at this flow rate calculated as 79.3%. The charging efficiency found increased to 82.5% when the flow rate increased to 6 LPM. The heat supplied and stored at this flow rate found to be 1044.6 kJ and 861.6 kJ respectively.

4.3 Discharging performance

To study the discharge performance of the PCM, the PCM is first charged to a temperature above the solid-solid transition point and then allowed to cool back to the ambient conditions. During the discharging process, the HTF at room temperature circulated through the heat exchanger. The PCM rejects the heat stored to the circulating HTF. The PCM temperature variation from the inlet to the exit of the heat exchanger in the axial direction recorded for evaluating the discharging performance of the PCM.

Figure 14 shows the temperature variation in the case of pure PE for HTF flow rates of 2, 4, and 6 LPM. The variation of the PCM temperature at six locations in the heat exchanger plotted in this figure. During the discharging, the PCM in the shell side of the heat exchanger rejects the heat to the HTF. The discharging process continued till all the temperatures recorded by the thermocouples recorded temperature equal to the ambient condition. The charging process ended in 106 minutes when a flow rate of 2 LPM maintained through the heat exchanger. The charging period found decreased to 86minutes and 65 minutes when the HTF flow rate changed to 4 LPM and 6 LPM respectively. The decrease in charging time observed was because of the increased heat absorption at the higher flow rates.

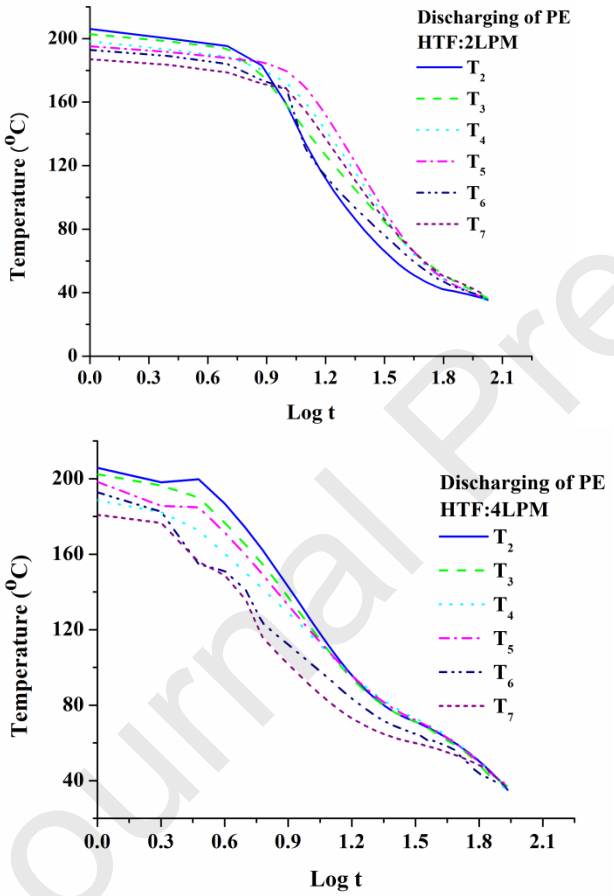

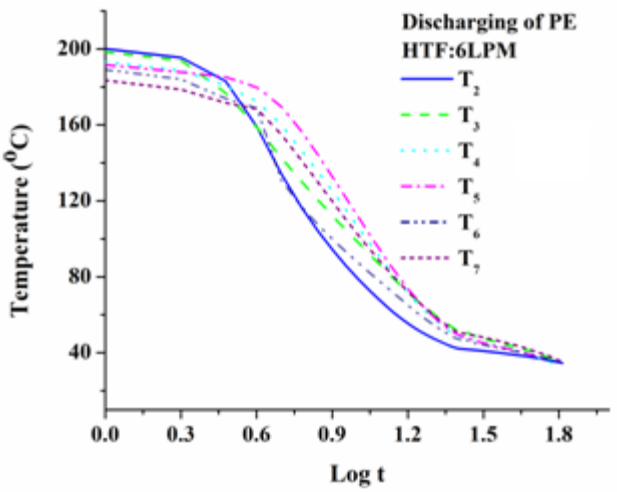

Figure 14: Discharging process of PE at different flow rates of HTF (HTF entry at T1, PCM temperatures- T2 to T7)

Figure 15 shows the temperature distribution in the PCM during the discharging process of PE added with 0.5 wt. % of LMA. The results showed that the discharging time of PE+0.5 wt.% LMA corresponding to the cold fluid rate of 2 LPM decreased from 106 minutes to 93 minutes. This indicated that the discharging time reduced by 12.3% due to the addition of 0.5 wt. % LMA. The discharging time found decreased to 75 minutes when the flow rate changed to 4 LPM indicating a 12.8% decrease. The discharge time further decreased to 57 minutes indicating a 12.3% decrease when the flow rate adjusted to 6LPM.

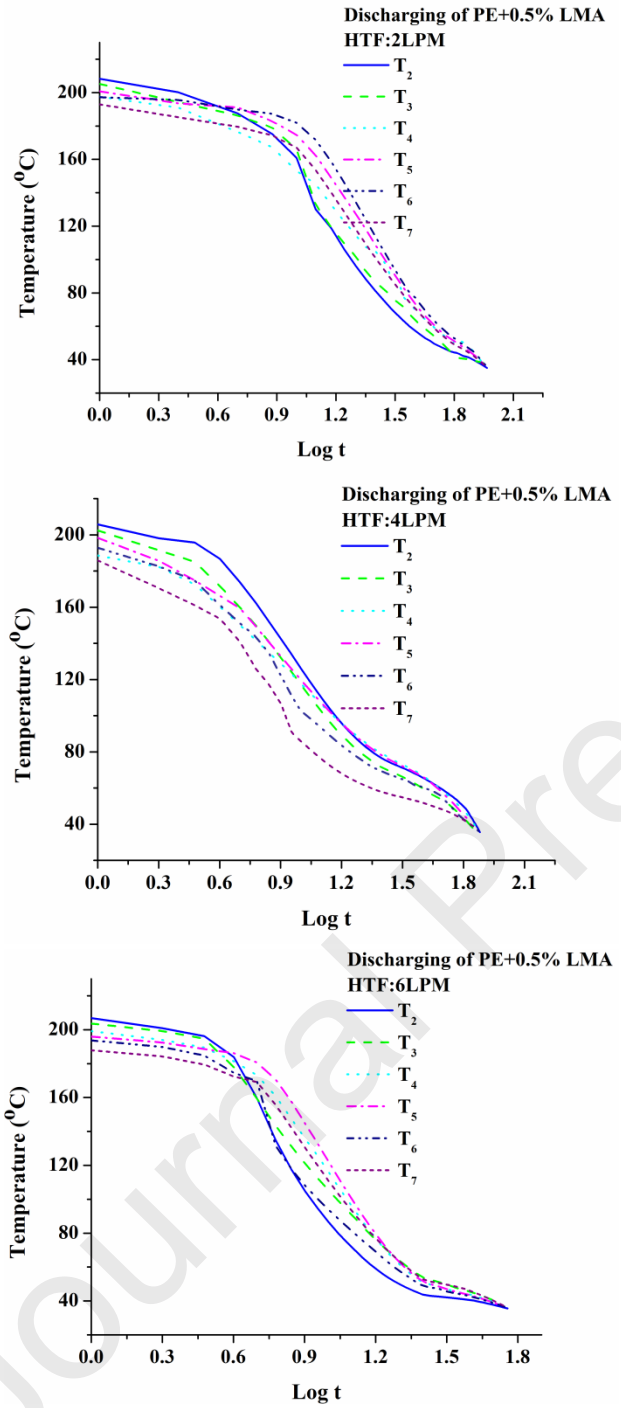

Figure 15: Discharging process of PE+0.5 wt. % LMA at different flow rates of HTF (HTF entry at T_1, PCM temperatures- T_2 to T_7)

Figure 16 shows the temperature distribution in the PCM during the discharging process of PE added with 1.0 wt. % of LMA. The results showed that the discharging time corresponding to the cold fluid rate of 2 LPM decreased from 106 minutes to 85 minutes. This indicated that the discharging time reduced by 19.8% due to the addition of 0.5 wt.

% LMA. The discharging time found decreased to 71 minutes when the flow rate changed to 4 LPM indicating a 17.4% decrease. The discharge time further decreased to 54 minutes indicating a 16.9% decrease when the flow rate adjusted to 6LPM. The % reduction in the discharging time of PE due to the addition of 0.5 and 1.0 wt.% of LMA summarized in figure 17.

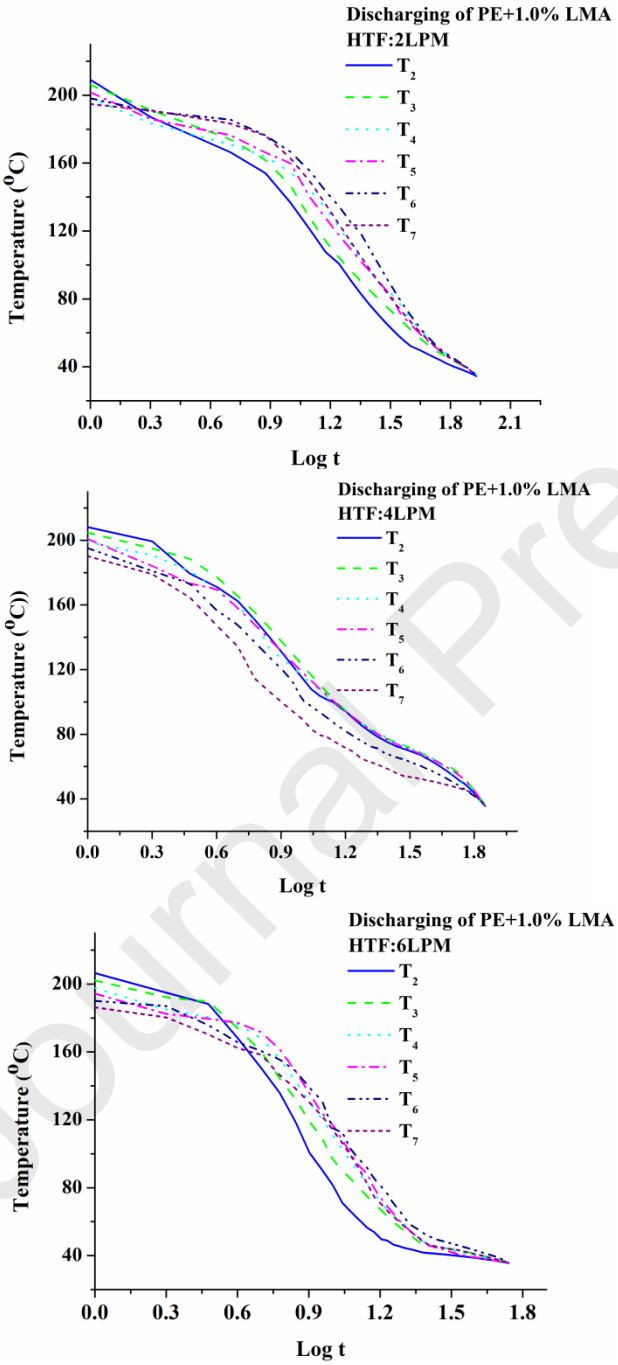

Figure 16: Discharging process of PE+1.0 wt. % LMA at different flow rates of HTF (HTF entry at T1, PCM temperatures- T2 to T7)

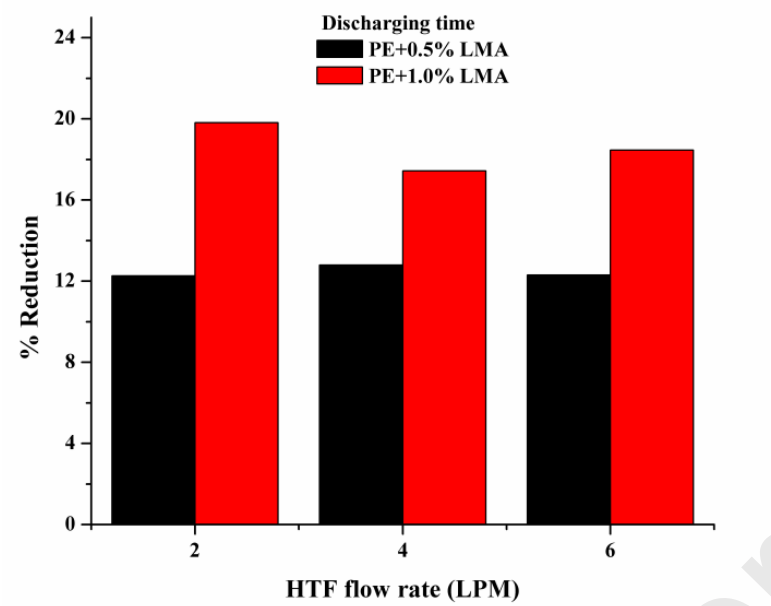

Figure 17: % reduction in discharging time of PE due to LMA at different HTF flow rates

4.4 Discharging power and efficiency

The average energy released per unit time to the circulating HTF estimated as the discharging power. Figure 18 shows the average discharging power estimated in the case of pure PE and PE added with 0.5 wt. % and 1.0 wt. % of LMA at different flow rates of the HTF.

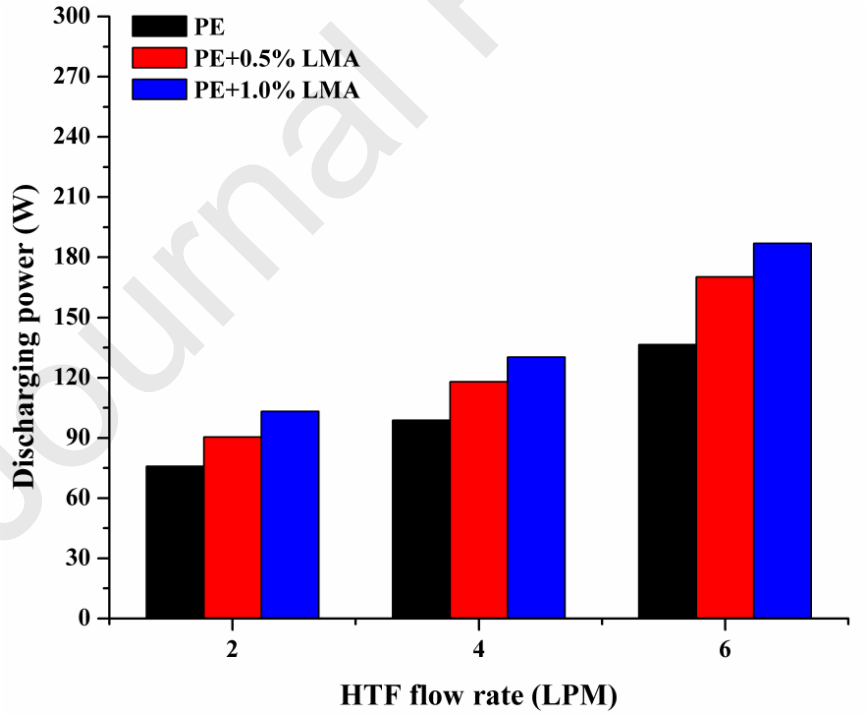

Figure 18: Average discharging power at different HTF flow rates

The experimental results showed that the discharging power of PE increases with the addition of additives for all the heating rates considered in this study. The average energy discharging power of pure PE corresponding to 2 LPM, 4 LPM, and 6 LPM flow rates estimated as 75.8 W, 98.8 W, and 136.5 W respectively. The results of the experiment conducted using PE added with 0.5 wt. % of LMA showed the average discharging power corresponding to 2 LPM, 4 LPM, and 6 LPM flow rates as 90.4 W, 117.9 W, and 170.2 W respectively. In the case of PE+1.0 wt.% LMA, the discharging power corresponding to 2, 4, and 6 LPM flow rates found to be 103.3 W, 130.3 W, and 187.0 W respectively.

The discharging efficiency is the ratio of heat absorbed by the HTF during the discharging cycle to the heat that was stored by the PCM during the charging cycle. Figure 19 shows the discharging efficiency obtained in the case of pure PE and PE added with 0.5 and 1.0 wt. % of LMA at different HTF flow rates. In the case pure PE, an amount of 482.2 kJ of energy discharged, out of the 916.4. kJ heat stored, at an HTF flow rate of 2 LPM. This indicated a discharging efficiency of 52.6%. When the flow rate changed to 4 LPM, 510.0 kJ of heat released to the HTF, out of 911.6 kJ of heat available. This accounts for a discharging efficiency of 55.9%. When the flow rate further increased to 6 LPM, the heat rejected to the HTF estimated as 532.2 kJ, out of 907.8 kJ heat stored by the PCM during the charging cycle. This gave a discharging efficiency of 58.6%.

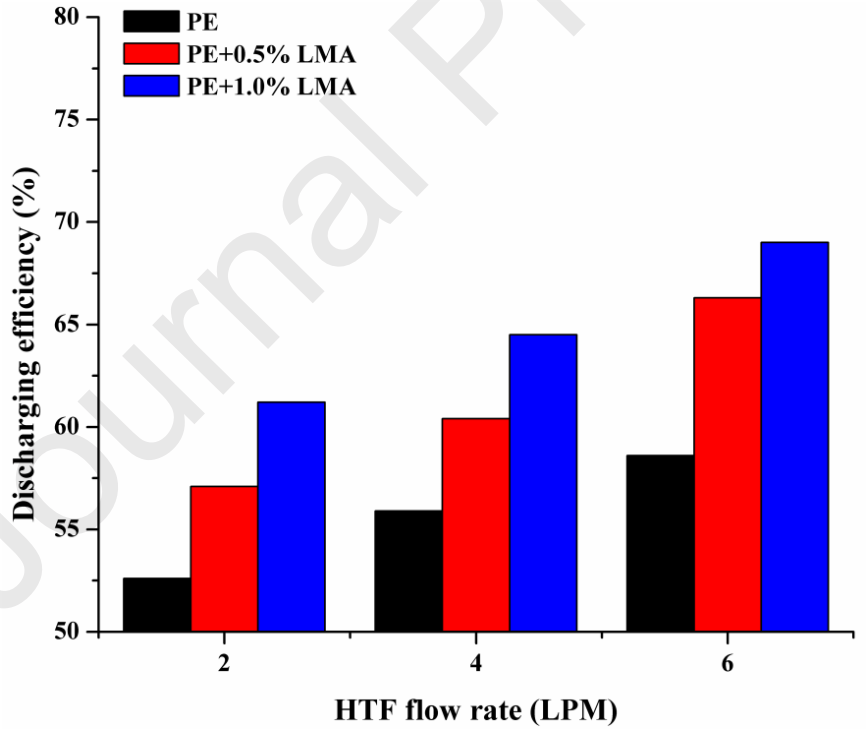

Figure 19: Discharging efficiency of PE with LMA at different flow rates

Figure 19 also shows the discharging efficiencies obtained in the case of PE added with 0.5 and 1.0 wt% of LMA. When 0.5 wt% of LMA added to PE, 504.5 kJ of heat

discharged, out of the 884.1 kJ of heat stored, to the HTF at 2 LPM. This indicated a discharging efficiency of 57.1%. When the flow rate changed to 4 LPM, 530.7 kJ of heat discharged to the HTF and the heat stored in the PCM during the previous charging cycle was 878.7 kJ. The discharging efficiency at this flow rate obtained as 60.4%.The discharging efficiency increased to 66.3% when the flow rate changed to 6 LPM. The energy available in the PCM and the energy released to the HTF at this flow rate found to be 877.5 kJ and 582.0 kJ respectively. The experimental results using PE+1.0 wt. % LMA indicated a discharging efficiency of 61.2% when a flow rate of 2 LPM maintained through the heat exchanger. The heat rejected to the HTF and the maximum heat that was available in the PCM corresponding to this flow rate found to be 527.0 kJ and 860.7 kJ respectively. When the HTF flow rate adjusted to 4 LPM, 555 kJ heat discharged, out of 860.0 kJ of heat that stored in the PCM during the previous charging period. The discharging efficiency at this flow rate calculated as 64.5%. The discharging efficiency increased to 69.0% when the flow rate increased to 6 LPM. The heat rejected and the heat stored in the PCM at this flow rate found to be 594.7 kJ and 861.6 kJ respectively.

4.5 Overall energy efficiency

The overall energy efficiency of the thermal energy storage (TES) system used in this experimental study calculated by combining the energy efficiencies computed separately for the charging and discharging processes. Figure 20 displays the overall efficiencies obtained using the different PCM samples for energy storage and release. The experimental results showed that the TES system using pure PE gave overall energy efficiencies of 34%, 38.5% and 42.3% corresponding to HTF flow rates of 2 LPM, 4 LPM, and 6 LPM respectively. The average efficiency of the system in the flow rate range 2-6 LPM was estimated to be 38.3%.

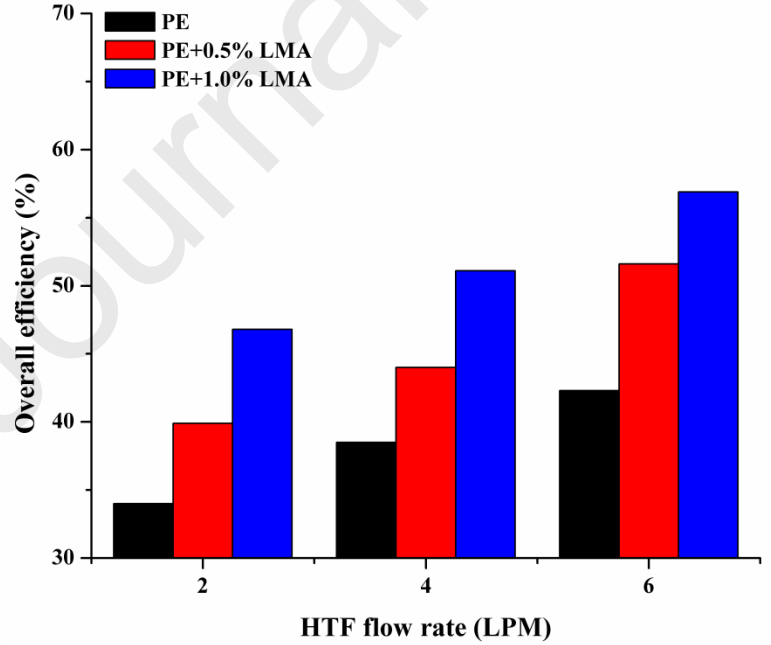

Figure 20: Overall energy efficiency of the thermal energy storage system at different HTF flow rates

It noted that the overall efficiency of the TES system also improved by the addition of LMA. In the case of PE+0.5wt. % LMA, the TES system showed overall energy efficiencies of 39.9%, 44.0%, and 51.6% corresponding to HTF flow rates of 2 LPM, 4 LPM, and 6 LPM. The average efficiency in the flow rate range of 2 to 4 LPM considered in this study obtained as 45.2%. The overall energy efficiencies of the TES system using PE+1.0wt.% LMA found to be 46.8%, 51.1%, and 56.9% when the HTF flow rates maintained were 2 LPM, 4 LPM, and 6 LPM respectively. The average energy efficiency of the TES system employing PE+1.0 wt. % LMA in the flow rate range of 2 to 4 LPM obtained as 51.6%.

The results of the experimental investigation discussed in the preceding sections reveals that the addition of LMA enhanced the thermal energy storage performance of pentaerythritol. The enhanced energy storage and release performance can be attributed to the improved thermal conductivity of PE due to the presence of conductive metal particles as reported in the section on thermal property measurement. The maximum value of the overall efficiency obtained corresponding to 1.0 wt. % of LMA at HTF flow rate of 6 LPM. This indicated that the charging and discharging occurs more efficiently at higher weight % of the additives and at higher flow rates of the HTF. Higher the weight % of LMA, greater is the enhancement in the thermal conductivity which resulted in the heat transfer at enhanced rate. The reason for the enhanced heat transfer occurred at the higher flow rate was because of the increased turbulence in the flow. The increased turbulence in region near to the tube wall caused very efficient fluid mixing and an efficient redevelopment of the thermal/hydrodynamic boundary layer leading to the improvement in the convective heat transfer [42-43].

Another noticeable thing in the results discussed in the previous sections was that the discharging efficiency found to be less than the charging efficiency at all flow rates of the HTF. This is because of the existence of subcooling in PE during the discharging cycle. Due to the subcooling effect, the soild-solid phase transition during the discharging cycle occurs at a temperature lower than the temperature at which the phase change occurs during the charging cycle. The result is that the quantity of heat discharged will be less than the quantity that is absorbed during the charging cycle. It can also be noted that the addition of LMA caused increase in the discharging efficiency. One of the major reasons for the increase was the enhanced heat transfer due to the improved thermal conductivity as mentioned earlier. In addition to the thermal conductivity enhancement, the presence of additives also reduced the subcooling effect leading to an increase in the quantity of heat discharged as observed at all HTF flow rates.. This means that the addition of LMA has a heterogeneous nucleation effect on the PE, and thus accelerates the solid-solid phase change process of PE. The LMA acted as the heterogeneous nucleation agent by

lowering the energy barrier toward nucleation. The degree of subcooling, which characterizes the overall rate of crystallization, decreased with the addition of LMA [32].

5. Experimental Uncertainties

The main parameter monitored during T-history, and thermal storage/release performance tests were the PCM and HTF temperatures. In this experimental study, K type thermocouples connected to a multi-channel data acquisition system (KEYSIGHT 34972A LXI) were used to record the various temperatures. The uncertainties in the energy measurements were calculated using the temperature and flow rate uncertainties. The uncertainties in the flow meter reading are specified by the manufacturer as $\pm$ 1% of full flow. The calibrated temperature sensors showed an uncertainty of ±0.1°C. Now the uncertainty in the heat supplied/recovered (δQ) was calculated using the know uncertainty values of temperature (δ_T) and mass flow rate of the HTF ($\delta_{\dot{m}}$). Therefore,

$$\delta Q = t c_{p,htf} \sqrt{(\Delta T\, \delta_{\dot{m}})^2 + 2\,(\dot{m}\, \delta_T)^2}$$

where, $\dot{m}$ −mass flow rate of the HTF,

$c_{p,htf}$ −specific heat of the HTF

ΔT –difference between the inlet and exit fluid temperatures

t- Time of charging/discharging

The uncertainty in the heat stored was estimated as $\delta Q_{stored} = M\, c_{p,pcm}\, (\Delta T \times \delta_T) + M\, (\delta_h)$, where δ_h is the uncertainty in the enthalpy change given by the DSC equipment and M is the mass of the PCM and $c_{p,pcm}$ is the specific heat of the PCM

Using the above relations, the uncertainties in heat supplied, heat stored and heat recovered in the HTF flow rate range considered in this work were estimated as 8.1%, 7.1%, and 8.5% respectively.

6. Summary and Conclusions

The charging and discharging performance of PE/LMA composite PCM containing 0.5 wt. % and 1.0 wt. % of LMA investigated in this experimental work. The following critical observations and conclusions are drawn. The time for charging of PE decreases due to the addition of 0.5 and 1 wt. % of LMA at all volume flow rates of the heat transfer fluid. The maximum reduction in the charging time of PE calculated to be 22.3%, 18.0% and 20.6% respectively corresponding to the therminol flow rates of 2, 4 and 6 LPM corresponding to 1.0 wt. % of LMA. The discharging time 2, 4 and 6 LPM flow rates of HTF reduced by 19.8%, 17.4%, and 16.9% respectively for PE+1,0 wt.% LMA. The reduction in the charging and discharging time observed is because of the increased rate of heat transfer because of the increased thermal conductivity of PE. The power and efficiency of charging and discharging of PE got improved by the incorporation of LMA. The maximum charging power and the maximum charging efficiency observed were 265.9 W and 82.5% respectively corresponding to the HTF flow rate of 6 LPM. The power and efficiency of discharging of PE improved by the presence of LMA. The maximum discharging power and the maximum discharging efficiency observed were 166.8 W and 69.0% respectively corresponding to the HTF flow rate of 6 LPM. The

mean value of the overall energy efficiency of the thermal energy storage (TES) system in the HTF flow rate range of 2 to 6 LPM found increased from 38.3% to 45.2 % and 51.6% corresponding to 0.5 wt. % and 1.0 wt. % respectively.

7. Acknowledgments

Authors express their sincere gratitude to Centre for Engineering Research and Development (KTU/RESEARCH 3/1199/2017 Dated 19.04.2017) for the financial assistance given for the execution of the work reported in this paper. In addition, the authors would like to acknowledge the funding acquired from UKIERI-DST (IND/CONT/GA/18-19/16), which made this research possible.

8. References

Wang Y, Liang D, Liu F, Zhang W, Di X, Wang C. A polyethylene glycol/hydroxyapatite composite phase change material for thermal energy storage. Applied Thermal Engineering. 2017 Feb 25;113:1475-82.

Amin M, Putra N, Kosasih EA, Prawiro E, Luanto RA, Mahlia TM. Thermal properties of beeswax/graphene phase change material as energy storage for building applications. Applied Thermal Engineering. 2017 Feb 5;112:273-80.

Jesumathy SP, Udayakumar M, Suresh S, Jegadheeswaran S. An experimental study on heat transfer characteristics of paraffin wax in horizontal double pipe heat latent heat storage unit. Journal of the Taiwan Institute of Chemical Engineers. 2014 Jul 1;45(4):1298-306.

A. Sharma, V. V. Tyagi, C. R. Chen, D. Buddhi, Review on thermal energy storage with phase change materials and applications, Renew. Sustainable Energy Rev. 13(2009) 318–345.

V.V. Tyagi, D. Buddhi, Thermal cycle testing of calcium chloride hexahydrate as a possible PCM for latent heat storage, Sol. Energy Mater. Sol. Cells 92(2008) 891–899.

R K Sharma, P Ganesan, V V Tyagi. Long-term thermal and chemical reliability study of different organic phase change materials for thermal energy storage applications. J Therm Anal Calorim 124(2016) 1357-66.

Zalba Belen, Jose Marin M, Cabeza Luisa F, Mehling Harald. Review on thermal energy storage with phase change: materials, heat transfer analysis and applications, Appl. Therm. Eng. 23(2003) 251–83.

S. Mondal, Phase change materials for smart textiles – an overview, Appl. Therm. Engg., 28 (2008) 1536–1550.

Fangyu Cao, Jing Ye, Bao Yang, Synthesis and Characterization of Solid-State Phase Change Material Microcapsules for Thermal Management Applications, J. Nanotechnol. Eng. Med. 4 (2013) 040901-1.

Benson, D.K., Webb, J.D., Burrows, R.W., McFadden, J. D. O., Christensen, C., 1985. Materials Research for Passive Solar Systems: Solid-State Phase Change Materials. Sol. Energy Res. Inst. SERI/TR-255- 1828.

Wang, X. W., Lu, E.R., Lin, W. X., Liu, T., Shi, Z. S., Tang, R. S., Wang, C. Z., 2000. Heat Storage Performance of the Binary Systems Neopentyl Glycol/Pentaerythritol and Neopentyl Glycol/Trihydroxy Methyl-Aminomethane as Solid-Solid Phase Change Materials. Energy Convers. Manage. 41, 129–134.

Xing, D. Q., Chi, G.S., Ruan, D.S., He, L.F., Li, D.H., Zhang, T.P., Zhang, D.S., 1995. Solid state phase transition in binary systems of polyhydric alcohols. Sol. Energy 16, 133–137.

Alkan, C., Gunther, E., Hiebler, S., Ensari, O. F., Kahraman, D., 2012. Polyurethanes as solid-solid phase change materials for thermal energy storage. Sol. Energy 86, 1761– 1769.

Gao, W.F., Lin, W.X., Liu, T., Xia, C.F., 2007. An experimental study on the heat storage performances of polyalcohols NPG, TAM, PE, and AMPD and their mixtures as solid-solid phase-change materials for solar energy applications. Int. J. Green Energy 4, 301–311.

Murrill, E., Breed, L. (1970) Solid-solid phase transitions determined by differential scanning calorimetry: Part I. Tetrahedral substances. Thermochimica Acta 1:239– 246.

Barrio, M., Font, J., Muntasell, J., Navarro, J., Tamarit, J. L., 1988. Applicability for Heat Storage of Binary Systems of Neopentylglycol, Pentaglycerine, and Pentaerythritol: A Comparative Analysis. Sol. Energy Mat. 18, 109-115.

Cheng F, Wen R, Huang Z, Fang M, Liu YG, Wu X, Min X. Preparation and analysis of lightweight wall material with expanded graphite (EG)/paraffin composites for solar energy storage. Applied Thermal Engineering. 2017 Jun 25;120:107-14.

Cheng F, Zhang X, Wen R, Huang Z, Fang M, Liu YG, Wu X, Min X. Thermal conductivity enhancement of form-stable tetradecanol/expanded perlite composite phase change materials by adding Cu powder and carbon fiber for thermal energy storage. Applied Thermal Engineering. 2019 Jun 25;156:653-9.

Praveen B, Suresh S, Pethurajan V. Heat transfer performance of graphene nano-platelets laden micro-encapsulated PCM with polymer shell for thermal energy storage based heat sink. Applied Thermal Engineering. 2019 Jun 25;156:237-49.

Adorno, A., Silva, R., 2006. Effect of Ag additions on the reverse martensitic transformation in the Cu- 10 mass% al alloy. J Therm. Anal. Calorim. 83, 241–6.

Siegel, R. (1977) 'Solidification of low conductivity material containing dispersed high

conductivity particles', International Journal of Heat and Mass Transfer, 20, 1087– 1089.

Cabeza, L.F., Mehling, H., Hiebler, S. and Ziegler, F. (2002) 'Heat transfer enhancement in water when used as PCM in thermal energy storage,' Appl. Therm. Engg., 22, 1141–1151.

Py, X., Olives, R. and Mauran, S. (2001) 'Paraffin/porous-graphite-matrix composite as high and constant power thermal storage material', International Journal of Heat and Mass Transfer, 44, 2727–2737.

Yin, H., Gao, X., Ding, J. and Zhang, Z. (2008) 'Experimental research on heat transfer mechanism of the heat sink with composite phase change materials', Energy Conversion and Management, 49, 1740–1746.

Kim, S. and Drzal, L.T. (2009) 'High latent heat storage and high thermal conductive phase change materials using exfoliated graphite nanoplatelets', Solar Energy Materials and Solar Cells, 93, 136–142.

Elgafy, A., Lafdi, K., 2005. Effect of carbon nanofibres additives on thermal behavior of phase change materials. Carbon 43, 3067–74.

Tun-Ping Teng, Chao-Chieh Yu, 2012. Characteristics of phase-change materials containing oxide nano-additives for thermal storage. Nanoscale Res. Lett. 7, 611.

Zhiwei Ge, Feng Ye, Hui Cao, Guanghui Leng, Yue Qin, Yulong Ding, 2014. Carbonate-salt-based composite materials for medium- and high-temperature thermal energy storage. Particuology 15, 77-81.

Xiang Li, Yuan Zhoua, Hongen Nian, Xinxing Zhang, Ouyang Dong, Xiufeng Ren, Jinbo Zeng, Chunxi Hai, Yue Shen, 2017. Advanced nanocomposite phase change material based on calcium chloride hexahydrate with aluminum oxide nanoparticles for thermal energy storage. Energy Fuels 3, 6560–6567.

D.K. Singh, S. Suresh, H. Singh, B.A.J. Rose, S. Tassou, N. Anantharaman, Myo-Inositol based nano-PCM for Solar Thermal Energy Storage, Appl. Therm. Engg., 110 (2017) 564–572.

M. Ghalambaz, A. Doostani, A. J.Chamkha, M. A.Ismael, Melting of nanoparticles-enhanced phase-change materials in an enclosure: Effect of hybrid nanoparticles, Int. Mech. Sci. 134(2017) 85-97.

N. H. Boukani, A. Dadvand, A. J.Chamkh, Melting of a Nano-enhanced Phase Change Material (NePCM) in partially-filled horizontal elliptical capsules with different aspect ratios, Int. Mech. Sci. 149 (2018) 164-177

Praveen B, Suresh S. Thermal performance of micro-encapsulated PCM with LMA thermal percolation in TES based heat sink application. Energy conversion and management. 2019 Apr 1;185:75-86.

P. Hu, P. P. Zhao, Y. Jin and Z. S. Chen, Experimental study on solid-solid phase change properties of pentaerythritol (PE)/nano-AlN composite for thermal storage, Sol. Energy 102 (2014) 91–97.

K P Venkitaraj, S Suresh (2019), Effects of Al_2O_3, CuO and TiO_2 nanoparticles on thermal, phase transition and crystallization properties of solid-solid phase change material, Mechanics of Materials, 128, pp. 64-88.

K P Venkitaraj, S Suresh (2018), Experimental study on the thermal storage performance and non-isothermal crystallization kinetics of pentaerythritol blended with low melting metal, Thermochimica Acta, 10, pp. 75-89

K P Venkitaraj, S Suresh, Arjun Venugopal, Experimental study on the thermal performance of nano-enhanced pentaerythritol in IC engine exhaust heat recovery application, Appl. Therm. Engg., 137 (2018) 461-474.

K.P. Venkitaraj, S Suresh (2017), Experimental study on thermal and chemical stability of pentaerythritol blended with low melting alloy as possible PCM for latent heat storage, Experimental Thermal and Fluid Science, 8, pp. 73-87.

Zhang Yinping, Jiang Yi and Jiang Yi, A simple method, the T –history method, of determining the heat of fusion, specific heat and thermal conductivity of phase-change materials, Meas. Sci. Technol. 10 (1999) 201–205.

Rezaei. M., Anisur M.R., Mahfuz M.H., Kibria, M.A., Saidur R., Metselaar. I.H.S.C. Performance and cost analysis of phase change materials with different melting temperatures in heating systems, Energy 53:173-178, 2013

S. Jagadheeswaran, S.D. Pohekar, T. Kousksou, Exergy based performance evaluation of latent heat thermal storage system: A review, Renewable and Sustainable Energy Reviews 14 (2010) 2580–2595.

M. Chandrasekar, S. Suresh, A. Chandra Bose, Experimental studies on heat transfer and friction factor characteristics of Al_2O_3/water nanofluid in a circular pipe under laminar flow with wire coil inserts, Experimental Thermal and Fluid Science 34 (2010) 122–130.

S. Suresh, K.P. Venkitaraj, P. Selvakumar, M. Chandrasekar, Effect of Al2O3–Cu/water hybrid nanofluid in heat transfer, Experimental Thermal and Fluid Science 38 (2012) 54– 60.

HIGHLIGHTS

Charging and discharging of pentaerythritol added with a low melt alloy

Energy storage performance of a shell and tube type thermal energy storage system

Reduced charging and discharging time of pentaerythritol by the low melt alloy

Increased charging and discharging power of pentaerythritol by low melt alloy

Enhanced charging and discharging efficiencies of PE due to low melting additive

Conflicts of interest: None

The authors declare that they have no known competing financial interests or personal relationships that could have appeared to influence the work reported in this paper.